Trapping of light with angular orbital momentum above the light cone in a periodic array of dielectric spheres

Evgeny Bulgakov[1,2] and Almas Sadreev[1]

[1]Kirensky Institute of Physics, Federal Research Center KSC SB RAS, 660036 Krasnoyarsk, Russia,
[2]Siberian State Aerospace University, Krasnoyarsk 660014, Russia
*corresponding author, E-mail: almas@tnp.krasn.ru

Abstract

We consider bound states in the radiation continuum (BSC) above the light cone in an one-dimensional periodic array of dielectric spheres in air. The BSCs are classified by orbital angular momentum m, Bloch wave vector β directed along the array, and polarization. The most simple symmetry protected BSCs have $m = 0, \beta = 0$ and occur in a wide range of the radius of spheres and dielectric constant. More sophisticated BSCs with $m \neq 0, \beta = 0$ exist only for a selected radius of the spheres at a fixed dielectric constant. We also show the existence of robust Bloch BSCs with $\beta \neq 0, m = 0$. The BSCs with $m = 0$ can be easily detected by the collapse of Fano resonance in scattering of a plane wave. In response to a plane wave with circular polarization the BSCs with $m \neq 0$ give rise to Poynting vector spiralling around the array.

1. Introduction

Recently guiding of electromagnetic waves by a linear array of dielectric spheres below the diffraction limit attracted considerable attention. There were two types of considerations: finite arrays [1, 2, 3, 4] and infinite arrays which were studied by means of the coupled-dipole approximation [5, 6, 7, 8, 9, 10]. A consummate analysis of electromagnetic waves propagating along linear arrays of dielectric spheres below the light cone was provided by Linton *et al* [11]. It is widely believed that only those modes whose eigenfrequencies lie below the light cone, are confined and the rest of the eigenmodes have finite life times. Recently confined electromagnetic modes above the light cone were shown to exist in various periodical arrays (i) of long dielectric cylindrical rods [12, 13, 14, 15, 17, 18], (ii) photonic crystal slabs [19, 20, 21, 22] and (iii) two-dimensional arrays of spheres [23]. Similarly, one may expect light trapping in the one-dimensional array of spheres with the bound frequencies *above light cone*. Such localized solutions of the Maxwell equations are known as the bound states in the continuum (BSC) and were first reported by von Neumann and Wigner [24]. The BSCs are of immense interest in optics thanks to experimental opportunity to confine light despite that outgoing waves are allowed in the surrounding medium [22, 25, 26, 27, 28, 29].

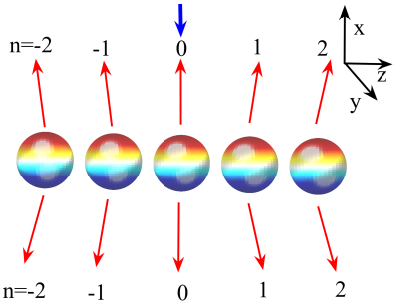

Figure 1: A periodic infinite array of dielectric spheres illuminated by a plane wave (blue arrow). The wave can be transmitted and reflected to discrete diffraction continua enumerated by integers m and n in accordance with Eqs. (8) and (12) shown by red arrows.

2. Basic equations for EM wave scattering by a linear array of spheres

We formulate the scattering theory for a periodic array of dielectric spheres in the form of the Lippmann-Schwinger equation similar to the approach developed for a periodic array of dielectric cylinders [15]

$$\widehat{L}\mathbf{\Psi} = \mathbf{\Psi}_{inc}. \tag{1}$$

Here the matrix $\widehat{L}$ is defined by the scattering matrix of the isolated sphere and mutual scattering events between the spheres, $\mathbf{\Psi}_{inc}$ is given by the incident wave, and the column $\mathbf{\Psi}$ is the solution of the scattering problem. It is the multipole expansion with TE and TM amplitudes a_l^m and b_l^m respectively where $l = 0, 1, 2, \ldots$ labels orbital momentum and $m = 0, \pm 1, \pm 2, \ldots$ enumerates its projection onto the z-axis which is the array axis as shown in Fig. 1. These amplitudes define the EM field in the form of an expansion over vector spherical harmonics $\mathbf{M}_n^m$ and $\mathbf{N}_n^m$ [11, 30]

$$\mathbf{E}(\mathbf{r}) = \sum_{j,lm} e^{i\beta\mathbf{R}_j}[a_l^m\mathbf{M}_l^m(\mathbf{r}-\mathbf{R}_j) + b_l^m\mathbf{N}_l^m(\mathbf{r}-\mathbf{R}_j)],$$

$$\mathbf{H}(\mathbf{r}) = -i\sum_j e^{i\beta\mathbf{R}_j}\sum_{lm}[a_l^m\mathbf{N}_l^m(\mathbf{r}-\mathbf{R}_j) + b_l^m\mathbf{M}_l^m(\mathbf{r}-\mathbf{R}_j)].$$

Here β is the Bloch wave vector directed along the array with $\mathbf{e}_z$ as the unit vector, $\mathbf{R}_j = j\mathbf{e}_z$ is the position of the

center of the j-th sphere, and the first/second terms presents TE/TM spherical vector EM fields. The exact expression of the matrix

$$\widehat{L} = \begin{pmatrix} \mathcal{A} & \mathcal{B} \\ \mathcal{B} & \mathcal{A} \end{pmatrix} \tag{2}$$

was derived by Linton *et al* [11] for EM guided waves on a periodic array of dielectric spheres. Mathematical expressions of matrix elements $\mathcal{A}_{l\nu}^{mm}$ and $\mathcal{B}_{l\nu}^{mm}$ are rather cumbersome. The reader can find explicit expressions in Refs. [11, 31].

The incident plane wave can be also expanded over vector spherical harmonics [30, 32]

$$\begin{aligned} \mathbf{E}^{\sigma}(\mathbf{r}) &= \textstyle\sum_{l=1}^{\infty}\sum_{-l}^{l}[q_{lm}^{\sigma}\mathbf{M}_l^m(\mathbf{r}) + p_{lm}^{\sigma}\mathbf{N}_l^m(\mathbf{r})], \\ \mathbf{H}^{\sigma}(\mathbf{r}) &= -i\textstyle\sum_{lm}[p_{lm}^{\sigma}\mathbf{M}_l^m(\mathbf{r}) + q_{lm}^{\sigma}\mathbf{N}_l^m(\mathbf{r})]. \end{aligned} \tag{3}$$

Here index σ stands for plane TE/TM wave.

$$\begin{aligned} p_{lm}^{TE} &= -F_{lm}\tau_{lm}(\alpha), \;\; q_{lm}^{TE} = F_{lm}\pi_{lm}(\alpha), \\ p_{lm}^{TM} &= -iF_{lm}\pi_{lm}(\alpha), \;\; q_{lm}^{TM} = iF_{lm}\tau_{lm}(\alpha), \end{aligned} \tag{4}$$

$k_x = -k_0\sin\alpha, k_y = k_0\cos\alpha,$

$$\begin{aligned} F_{lm} &= (-1)^m i^l\sqrt{\tfrac{4\pi(2l+1)(l-m)!}{(l+m)!}}, \\ \tau_{lm}(\alpha) &= \tfrac{m}{\sin\alpha}P_l^m(\cos\alpha), \\ \pi_{lm}(\alpha) &= -\tfrac{d}{d\alpha}P_l^m(\cos\alpha). \end{aligned} \tag{5}$$

For a particular case of normal incidence $k_z = 0, \alpha = -\pi/2$ we obtain from Eqs. (5)

$$\tau_{lm} = -mP_l^m(0), \pi_{lm} = -\frac{d}{d\alpha}P_l^m(0). \tag{6}$$

The general equation for the amplitudes a_l^m, b_l^m which describe the scattering by a linear array of spheres takes the following form

$$\begin{aligned} Z_{TE,l}^{-1}a_l^m - \textstyle\sum_{\nu}(a_\nu^m\mathcal{A}_{\nu l}^{mm} + b_\nu^m\mathcal{B}_{\nu l}^{mm}) = q_{lm}^{\sigma}, \\ Z_{TM,l}^{-1}b_l^m - \textstyle\sum_{\nu}(a_\nu^m\mathcal{B}_{\nu l}^{mm} + b_\nu^m\mathcal{A}_{\nu l}^{mm}) = p_{lm}^{\sigma}. \end{aligned} \tag{7}$$

3. The diffraction continua of vector cylindrical modes

Thanks to the axial symmetry of the array we can exploit the vector cylindrical modes for description of the diffraction continua which are doubly degenerate in TM and TE polarizations σ. The modes can be expressed through a scalar function ψ [30]

$$\psi_{m,n}(r,\phi,z) = H_m^{(1)}(\chi_n r)e^{im\phi + ik_{z,n}z}. \tag{8}$$

Then for the TE modes we have [30]

$$\begin{aligned} E_z &= 0, \;\; H_z = \psi_{m,n}, \\ E_r &= \tfrac{ik_0}{\chi_n^2}\tfrac{1}{r}\tfrac{\partial\psi_{m,n}}{\partial\phi}, \;\; H_r = \tfrac{ik_z}{\chi_n^2}\tfrac{\partial\psi_{m,n}}{\partial r}, \\ E_\phi &= \tfrac{-ik_0}{\chi_n^2}\tfrac{\partial\psi_{m,n}}{\partial r}, \;\; H_\phi = \tfrac{ik_z}{\chi_n^2}\tfrac{1}{r}\tfrac{\partial\psi_{m,n}}{\partial\phi}, \end{aligned} \tag{9}$$

and for the TM modes

$$\begin{aligned} E_z &= \psi_{m,n}, \;\; H_z = 0, \\ E_r &= \tfrac{ik_z}{\chi_n^2}\tfrac{\partial\psi_{m,n}}{\partial r}, \;\; H_r = \tfrac{-ik_0}{\chi_n^2}\tfrac{1}{r}\tfrac{\partial\psi_{m,n}}{\partial\phi}, \\ E_\phi &= \tfrac{ik_z}{\chi_n^2}\tfrac{1}{r}\tfrac{\partial\psi_{m,n}}{\partial\phi}, \;\; H_\phi = \tfrac{ik_0}{\chi_n^2}\tfrac{\partial\psi_{m,n}}{\partial r}, \end{aligned} \tag{10}$$

where

$$\chi_n^2 = k_0^2 - k_{z,n}^2 \tag{11}$$

and

$$k_{z,n} = \beta + 2\pi n, \;\; n = 0, \pm1, \pm2, \ldots. \tag{12}$$

General theory of scattering in terms of the amplitudes $\mathbf{\Psi} = (a_l^m, b_l^m)$ is formulated in the form of Eq. (7) which allows to find the amplitudes via the inverse of the matrix $\widehat{L}$

$$\mathbf{\Psi} = \widehat{L}^{-1}\mathbf{\Psi}_{inc}. \tag{13}$$

This equation is the Green equation in which a source presented by incident wave $\mathbf{\Psi}_{inc}$ unambiguously gives the solution as the scattered wave $\mathbf{\Psi}$. There is however a unique case when the solution of linear equation (1) is not unambiguous [37] when the inverse of the matrix $\widehat{L}$ does not exists for $Det(\widehat{L}) = 0$ [38, 39]. That occurs if one of complex eigenvalues of $\widehat{L}$ turns to zero giving rise to the BSC as a null eigenvector of $\widehat{L}$

$$\widehat{L}\mathbf{\Psi}_{BSC} = 0. \tag{14}$$

The necessary and sufficient condition for the BSC is orthogonality of $\mathbf{\Psi}_{BSC}$ to the right hand of Eq. (1) [39]. In other words, the BSC occurs when the coupling of the solution of Eq. (1) with continuum turns to zero [40]. Then the solution of Eq. (7) can be presented as linear superposition of the BSC and the particular solution [38, 39]

$$\mathbf{\Psi} = \alpha\mathbf{\Psi}_{BSC} + \mathbf{\Phi} \tag{15}$$

where α is an arbitrary constant.

In what follows we consider the BSCs in the diffraction continua specified by two quantum numbers m and n where the m is the result of the axial symmetry and n is the result of translational symmetry of the infinite linear array of the dielectric spheres. Note that each diffraction continuum is doubly degenerate relative to the polarization σ. The interplay between the frequency k_0 and the wave number $k_{z,n}$ the continua can be open (χ is real) or closed (χ is imaginary). In the present paper we restrict ourselves by the case of one, two and three open continua.

One can ask themselves why BSCs can occur in periodic dielectric structures but not in homogeneous structures like a slab or a rod which can only support guided EM modes below the light cone. Let us begin with the simplest textbook system of dielectric slab infinitely long in the x, y plane with the dielectric constant $\epsilon > 1$. The Maxwell equations can be solved by separation of variables for scalar function $\psi(x,y,z) = e^{ik_x x + ik_y y}\psi(z)$ to result in bound states below the light cone $k_0^2 = k_x^2 + k_y^2$

[41]. The situation can be cardinally changed if the continual translational symmetry is replaced by the discrete one $\epsilon(x,y,z) = \epsilon(x+ph,y,z)$ where $p = 0, \pm1, \pm2, \ldots$, h is the period of the structure. Then the radiation continua are quantized $k_{x,n} = \beta + 2\pi n/h,\ \ n = 0, \pm1, \pm2, \ldots$ and are given by outgoing plane waves $e^{ik_{x,n}x+ik_y y+ik_z z}$ with the frequency $k_0^2 = k_{x,n}^2 + k_y^2 + k_z^2$, where β is the Bloch wave vector along the x-axis and the integer n refers to diffraction continua [14].

Physical interpretation of this statement is related to that the slab with discrete translational symmetry can be considered as one-dimensional diffraction lattice. Let us take for simplicity $\beta = 0, k_y = 0$. Assume there is a bound solution with the eigenfrequency $k_{0BSC} > 0$ which is coupled with all diffraction continua enumerated by n. Let $k_{0BSC} < 2\pi/h$, i.e., the BSC resides in the first diffraction continua but below the others. Because of the symmetry or by variation of the material parameters of the modulated slab we can achieve that the coupling of the solution with first diffraction continuum equals zero [15, 17, 20, 21, 22]. However the solution is coupled with continua $n = 1, 2, \ldots$ which are evanescent that give rise to exponential decay of the solution over z-axis. The length of localization $L \sim \frac{1}{\sqrt{2\pi^2/h^2 - k_{0BSC}^2}}$. Therefore the evanescent diffraction continua play a principal role in the space configuration of the BSCs because they establish the EM fields in the near zone of the array beyond the dielectric rods or spheres.

For the present case of the infinite periodical array of dielectric spheres the diffraction continua are given by Eqs. (11) and (12). For the lowest continuum $n = 0$ and for $m = 0, \beta = 0$ (standing BSC) the corresponding cylindrical mode of the continuum (8) is constant along the array axis z. Then for given radius and permittivity of the spheres one can find symmetrical solutions which have zero overlapping with this continuum mode because of the symmetry of the solution. Examples of such a symmetry protected BSCs of both pure polarizations are given in Fig. 2. The BSCs exist in a wide range of material parameters as was established by Lu and Yuan for the array of dielectric rods [42]. However the cases of BSCs with $m \neq 0$ or with mixed polarizations need special numerical analysis and will be presented below.

4. Symmetry classification of BSCs

There might be two kinds of the bound modes which are the solutions of the homogeneous Eq. (14). The first type of modes below the light cone have wave number $\beta > k_0$ and describe guided waves along the array. These solutions found by Linton *et al* exist in some interval of material parameters of spheres, dielectric constant ϵ or radius R and the Bloch wave number β [11]. The second type of bound modes have wave numbers $\beta < k_0$ embedded into the diffraction continua above the light cone (BSCs). It is much more difficult to establish the existence of the second type of bound states because of tuning of material parameters. However there are a class of symmetry protected BSC

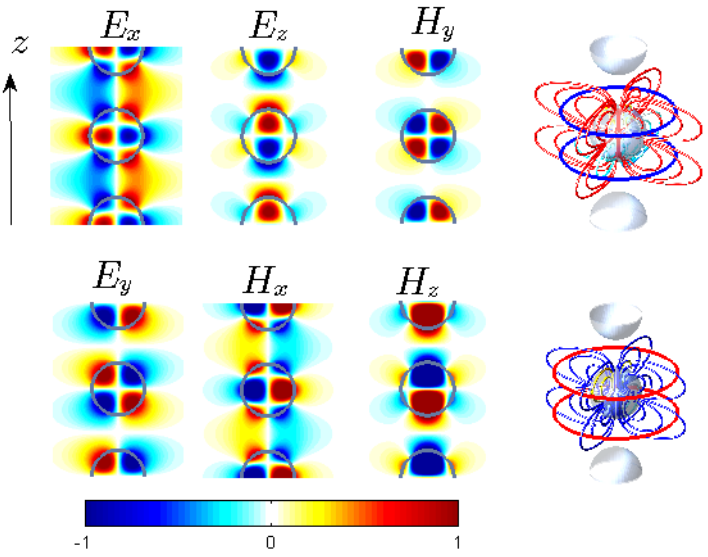

Figure 2: Patterns of the symmetry protected TM BSC (up) and TE BSC (down) with $m = 0$. Electric force lines are in red and magnetic force lines are in blue. Green solid lines show spheres.

which are free of tuning of the material parameters but exist only for selected values of Bloch vector β [42]. These BSC have been already considered in the linear array of infinitely long dielectric rods [12, 14, 15, 16, 20, 22, 26].

First, axial symmetry of the array implies that the matrixes $\mathcal{A}$ and $\mathcal{B}$ split over the irreducible representations of magnetic quantum number m which therefore classifies the BSCs. Second, discrete translational symmetry along the z-axis implies that respective wave vector component β specifies the BSC with discrete k_0 too. At last, additional optional symmetries arise due to the inversion symmetry transformation $\widehat{K}f(x,y,z) = f(x,y,-z)$ for $\beta = 0, \pi$. The selection rules for the amplitudes $a_l^m,\ b_l^m$ were established in Ref. [31] and listed in 1. In turn, the symmetry properties of the cartesian components of vector spherical functions under the inversion of z allow to establish the symmetric properties of EM fields collected in Table II.

Table 1: Classification of the BSCs.

m	β	I type of BSC	II type of BSC
$\neq 0$	0	$(a_{2k}^m,\ b_{2k+1}^m)$	$(a_{2k+1}^m,\ b_{2k}^m)$
0	$\neq 0$	$(a_l^0,\ 0), E_z = 0$	$(0,\ b_l^0), H_z = 0$
0	0	$(a_{2k}^0,\ 0), E_z = 0$	$(0,\ b_{2k}^0), H_z = 0$
0	0	$(0,\ b_{2k+1}^0), H_z = 0$	$(a_{2k+1}^0,\ 0), E_z = 0$

Light can be trapped above the light cone due to the most simple symmetry mechanism in symmetry protected BSCs with $m = 0, \beta = 0$. They constitute the majority of the BSCs. The symmetry-protected BSCs are either pure TE spherical vector modes (Type I in Table I) which are pure TE spherical vector modes (the I type in Table I) with

Table 2: Symmetry properties of the eigenmodes for $\beta = 0$.

I type	II type
$E_{x,y}(-z) = (-1)^{m+1}E_{x,y}(z)$	$E_{x,y}(-z) = (-1)^{m}E_{x,y}(z)$
$E_{z}(-z) = (-1)^{m}E_{z}(z)$	$E_{z}(-z) = (-1)^{m+1}E_{z}(z)$
$H_{x,y}(-z) = (-1)^{m}H_{x,y}(z)$	$H_{x,y}(-z) = (-1)^{m+1}H_{x,y}(z)$
$H_{z}(-z) = (-1)^{m+1}H_{z}(z)$	$H_{z}(-z) = (-1)^{m}H_{z}(z)$

$a^0_{2k} \neq 0, b^0_k = 0$ and TM spherical vector modes (the II type) with $a^0_k = 0, b^0_{2k} \neq 0$. Numerical results for the coefficients a_l, b_l are given in Ref. [31]. Here we show only two examples of the symmetry protected BSCs, one the TE BSC in Fig. 2 (a) and second the TM BSC in Fig. 2 (b). Note the profiles are periodic over the chain. Hereinafter we plot real parts of electromagnetic fields.

5. Robust Bloch BSCs with $\beta \neq 0, m = 0$

Could the Bloch BSC occur at $\beta \neq 0$ in the continuum of free-space modes? This question was first answered positively by Porter and Evans [33] who considered acoustic trapping in the array of rods of rectangular cross-section. Marinica *et al* [13] demonstrated the existence of the Bloch BSC with $\beta \neq 0$ in two parallel dielectric gratings and Ndangali and Shabanov [14] in two parallel arrays of dielectric rods. In a single array of rods positioned on the surface of bulk 2d photonic crystal multiple BSCs with $\beta \geq 0$ were considered by Wei *et al* [20]. Also the Bloch BSCs in a single array of cylindrical dielectric rods in air were presented in Refs. [15, 42]. Only the solution with Bloch vector β_c is true Bloch BSC. As soon as β deviates from this point the quasi Bloch BSC will decay losing the power for propagating. Therefore narrow wave packets centered around the the BSC frequency are capable to guide the EM power rather long distances [43] with the group velocity $dRe(\omega(k))/dk$.

According to Table I the Bloch BSCs with $\beta \neq 0, m = 0$ have only components a^0_l or b^0_l. Let us first consider the type I of BSC with $b^0_l = 0$ which has $E_z = 0$ and, therefore, is decoupled with the TM continuum but is coupled with the TE $n = 0, m = 0$ continuum. By solving the equation for complex eigenvalues of the matrix (7) and searching for the case when one of them turns to zero we achieve a vanishing coupling [40] under variation of β. Then the corresponding eigenvector, column of amplitudes a_{lm} and b_{lm} gives us the pattern of EM fields shown in Fig. 3 after substitution them into Eq. (2). One can see that the solution has no periodicity.

This BSC occurs under variation β but there is no necessity to tune material parameters of the spheres and therefore the BSC can be still defined as robust which is attractive from the experimental point of view. We managed to find only the type I of the BSCs for $\epsilon = 15$ but not the type II. Such a difference between types of the BSC is related to different boundary conditions for electric and magnetic fields at the dielectric sphere.

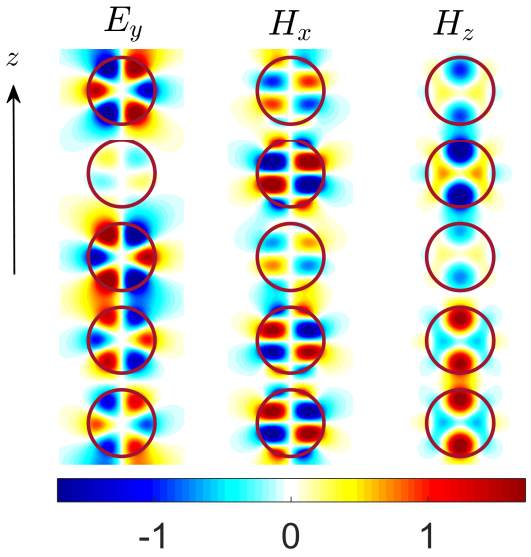

Figure 3: (Color online). EM field configurations of the Bloch BSC with $\beta = 1.2074$.

6. Orbital angular momentum BSCs

The BSCs with orbital angular momentum (OAM) $m \neq 0$ are of primary interest in the present paper. The mechanism for partially symmetry protected BSCs allows us to understand how to realize the BSCs with $m \neq 0, \beta = 0$ which are embedded into the diffraction continuum with the same m and $n = 0$. Obviously, the system has the time reversal symmetry that implies that such BSCs are degenerate with the respect to the sign $\pm m$. Let us start with the BSC of the I type with $m = 1$ which has the odd E_z and the even H_z according to Tables I and II. The diffraction TE and TM modes $m = 1, n = 0$ are independent of z and therefore as it follows from Eqs. (9) and (10) the solutions of type I are mismatched with the TM continuum but are coupled with the TE continuum. The coupling was cancelled by the same numerical procedure as described in the previous section now by tuning the radius of the spheres. The results of computation of this partially symmetry protected BSC of type I (a_{2k}, b_{2k+1}) are given in Ref. [31] and shown in Fig. 4 (a) for $m = 1$.

The next type of BSC (a_{2k+1}, b_{2k}) with $m = 2$ belongs to type II with even E_z and odd H_z. It is symmetry protected against decay into the TE continuum with $m = 2, n = 0$. The decay into the TM continuum is can be eliminated by tuning the sphere radius and shown in Fig. 4 (b). All components of electric and magnetic fields of the BSCs are nonzero and localized around the array [31] similar to that shown in Fig. 2. Here we show only force lines of EM fields around one sphere because patterns are periodic along the z-axis. The value of OAM m reflects the structure of force lines in the xy-plane while number of sufficient amplitudes in orbital momentum l reflects in the structure along the z-axis.

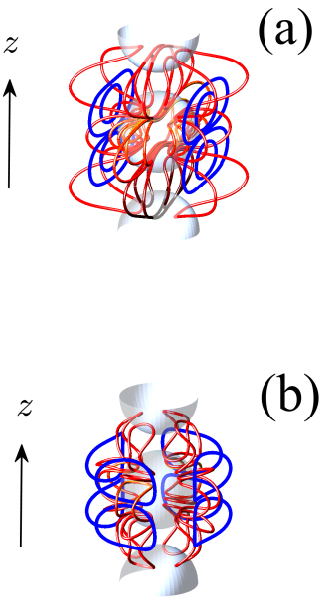

Figure 4: Electric force (red) and magnetic force (blue) lines BSCs with OAM (a) $m = \pm 1$ and (b) $m = \pm 2$.

7. Emergence of the BSC in scattering

Scattering of plane waves by periodic two-dimensional arrays of dielectric spheres has been in focus of researches since pioneering papers by Ohtaka *et al* [34]. Scattering by aggregates of finite number of spheres was considered in the framework of multisphere Mie scattering [32, 35, 36], however to our knowledge the scattering by the one-dimensional infinite array of dielectric spheres has not been considered yet. This section aims to present the results of numerical calculation of differential and total cross-sections of the infinite array with the focus on the resonant traces of the BSCs in the cross-sections similar to the scattering by array of dielectric rods [15, 20, 22]. As soon as one deviates from the BSC point the BSC manifests in the form of collapsing Fano resonance for approaching to the BSC point in parametric space. That phenomenon was observed in scattering of EM waves by arrays of rods [14, 15, 16, 20, 22, 23]. The Fano resonance for the present system can be interpreted as interference of two paths, one through the spheres and one between the spheres. In what follows we present briefly a mathematical tool to highlight these features of the BSCs using the biorthogonal basis of eigenvectors of the non Hermitian matrix $\widehat{L}$ [15, 44]

$$\widehat{L}\mathbf{X}_f = L_f\mathbf{X}_f, \;\; \widehat{L}^+\mathbf{Y}_f = L_f^*\mathbf{Y}_f, \;\; \mathbf{Y}_f^+\mathbf{X}_{f'} = \delta_{ff'}. \quad (16)$$

It immediately follows that

$$\widehat{L}^{-1} = \sum_f \mathbf{X}_f \frac{1}{L_f}\mathbf{Y}_f^+. \quad (17)$$

Because of axial symmetry the matrix (7) has the block structure

$$L_{ll'}^{(m)} = \begin{pmatrix} Z_{TE,l}^{-1}\delta_{ll'} - \mathcal{A}_{ll'}^{mm} & -\mathcal{B}_{ll'}^{mm} \\ -\mathcal{B}_{ll'}^{mm} & Z_{TM,l}^{-1}\delta_{ll'} - \mathcal{A}_{ll'}^{mm} \end{pmatrix}. \quad (18)$$

In the nearest vicinity of the BSC point one of the complex eigenvalues L_c is very close to zero. That allows us to substantially simplify Eq. (17) leaving in the sum only the leading contribution related to the L_c. Respectively the scattering state in Eq. (13) is simplified as follows

$$\mathbf{\Psi}^\sigma \approx \frac{1}{L_c}\mathbf{X}_c(\mathbf{Y}_c^+ \cdot \mathbf{\Psi}_{inc}^\sigma), \quad \sigma = TE/TM. \quad (19)$$

This equation manifests a remarkable property of the BSCs to enhance the incident wave $\mathbf{\Psi}_{inc}$ by the factor $1/L_c$. First we present this effect for the symmetry protected BSCs with $m = 0$ shown in Fig. 2 when a plane wave with the wave vector in plane x, z and TE polarizations with electric field along the y-axis illuminates the array. The small complex eigenvalue L_c in the denominator of scattering wave function (19) results in sharp resonant contribution in the cross-section $\sigma_{TE,TE}$ as shown in Fig. 5 (a). When the plane wave is incident normally to the array of the spheres $k_z = 0$ (dash line) the BSC of type I is fully invisible in the cross-section. Alternatively, the symmetry protected type II of the symmetry protected BSCs with the only amplitudes b_k can be observed via the cross-section $\sigma_{TM\to TM}$ which shows similar anomalies in the cross-section $\sigma_{TM,TM}$ as seen from Fig. 5 (b). Thus, although the BSCs have no effect for the normal incidence they are detected by collapse of Fano resonances in total cross-sections for $k_z \to 0$.

8. Transfer of spin momentum of circularly polarized wave into orbital momentum of the BSC with $m \neq 0$

Scattering of circularly polarized plane wave by the OAM BSCs is the main issue of the this section. It is well known that EM fields can carry not only energy but also angular momentum. The angular momentum is composed of spin angular momentum (SAM) and OAM describing its polarization state and the phase structure distribution, respectively. The research on OAM of EM fields attracted attention since Allen *et al.* investigated the mechanism of OAM in laser modes [45, 46]. In contrast to SAM, which has only two possible states of left-handed and right-handed circular polarizations, the theoretical states of OAM are unlimited owing to its unique characteristics of spiral flow of propagating EM waves [47]. There were many proposals to generate OAM beams by use of ferrite particles [48], by chiral plasmonic nanostructures [49] and by designer metasurfaces [50]. Here we show that the BSCs with OAM are capable to generate spinning currents in response to illumination of the array by circularly polarized plane wave.

Because of time-reversal symmetry BSCs with OAM are degenerate in the sign of m. That modifies Eq. (19) as

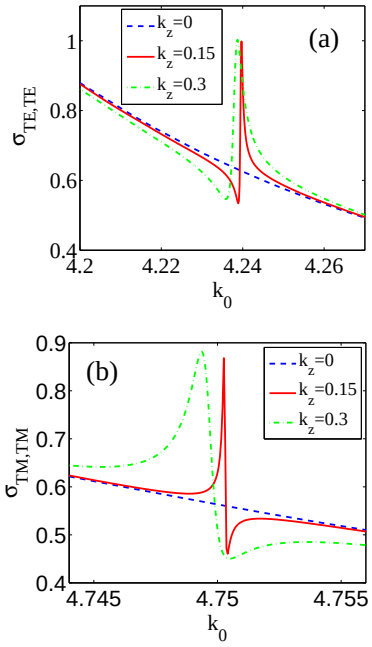

Figure 5: Total cross-section for scattering of TE (a)/TM (b) plane wave incident under angle to the array of dielectric spheres strongly effected by presence of the symmetry protected type I/II BSC shown in Fig. 2 (a).

follows

$$\mathbf{\Psi}_{\sigma}^{m} \approx \frac{1}{L_c}\sum_{\pm}[\mathbf{X}_c(\pm m)(\mathbf{Y}_c(\pm m)^{+}\cdot\mathbf{\Psi}_{inc}^{\pm m,\sigma})] \quad (20)$$

where the incident wave according to Eq. (7) is given

$$\mathbf{\Psi}_{inc}^{m,\sigma} = \begin{pmatrix} \mathbf{p}_m^{\sigma} \\ sgn(m)\mathbf{q}_m^{\sigma} \end{pmatrix}, \quad (21)$$

and subvectors $\mathbf{p}^m$ and $\mathbf{q}^m$ are given by Eqs. (4). From Eq. (18) and property $\mathcal{B}_{ll'}^{(m)} = -\mathcal{B}_{ll'}^{(-m)}$ the eigenvectors can be decomposed over the polarizations as follows

$$\mathbf{X}_c(\pm m) = \begin{pmatrix} \mathbf{x}_{TE}^m \\ \pm\mathbf{x}_{TM}^m \end{pmatrix}, \mathbf{Y}_c(\pm m) = \begin{pmatrix} \mathbf{y}_{TE}^m \\ \pm\mathbf{y}_{TM}^m \end{pmatrix}. \quad (22)$$

As a result substitution of Eqs. (21) and (22) into Eq. (20) gives

$$\mathbf{\Psi}_{\sigma} \approx \frac{1}{L_c} D_{\sigma}(\mathbf{X}_c^{+m} \pm \mathbf{X}_c^{-m}) \quad (23)$$

where the sign $\pm$ refers to the TE/TM polarizations and

$$D_{\sigma} = \mathbf{y}_{TE}^{+}\mathbf{p}_{|m|}^{\sigma} + \mathbf{y}_{TM}^{+}\mathbf{q}_{|m|}^{\sigma}. \quad (24)$$

Asymptotically $D_{TM} \to 0$ for $k_z \to 0$. Assume that the elliptically polarized plane wave $\mathbf{\Psi}_{inc}^{TE} + \alpha\mathbf{\Psi}_{inc}^{TM}$ is incident almost normally to the array with small k_z. Instantly from Eq. (23) we obtain that

$$\mathbf{\Psi}_{\sigma} \approx F\mathbf{X}_c^{+m}, F = \frac{2D_{TE}}{L_c} \quad (25)$$

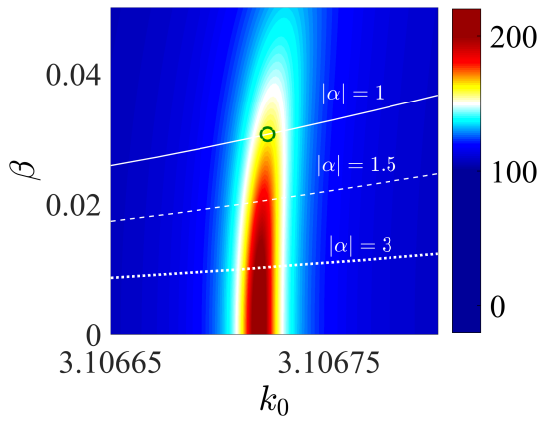

Figure 6: The enhancement factor $|F|$ vs frequency and k_z. The parameter α controls polarization of incident wave $\mathbf{\Psi}_{inc}^{TE} + \alpha\mathbf{\Psi}_{inc}^{TM}$. Open circle marks point $\beta = 0.0306, k_0 = 3.1067$.

for

$$D_{TE} = \alpha D_{TM} \quad (26)$$

the scattering wave function has only a contribution with the positive OAM $m > 0$. Here we introduced the enhancement factor F which defines to what extent the incident wave amplitude enhances near by the array. Respectively for $D_{TE} = -\alpha D_{TM}$ the scattering wave function has only a contribution with the negative OAM $m < 0$. Fig. 6 illustrates the behavior of the enhancement factor in the plane of the frequency k_0 and β for elliptically polarized plane waves with the polarization parameter α. In particular $\alpha = -0.3133 + i0.9496$ corresponds to the circularly polarized wave.

Let us examine the scattering wave function as we bypass the BSC point $\omega_{BSC} = 3.086, R = 0.471, \epsilon = 15$ shown in Fig. 4 (b) where the radius of spheres is measured in terms of the period of the array. The solution for the BSC with $m = 2$ is the following [31]

$$(a_l^2,\, b_l^2) = \begin{pmatrix} 0 & 0.6545 + 0.2013i \\ -0.2142 + 0.6964i & 0 \\ 0 & -0.0057 - 0.0018i \\ 0 & 0 \\ 0 & 0 \end{pmatrix} \quad (27)$$

where $l \geq 2$. In what follows we take $R = 0.468$ and sweep the frequency of incident wave k_0 in the nearest vicinity of the BSC frequency 3.086. Then because of smallness of the eigenvalue L_c in Eq. (23) EM fields given by the scattering wave function can reach high values near the spheres. It is clearly a property of the extremely high quality of the BSCs, that presents a possibility to enhance the incident light [23, 16] that is illustrated in Fig. 7 (a). Besides carrying OAM the BSC with $m \neq 0$ provide an opportunity

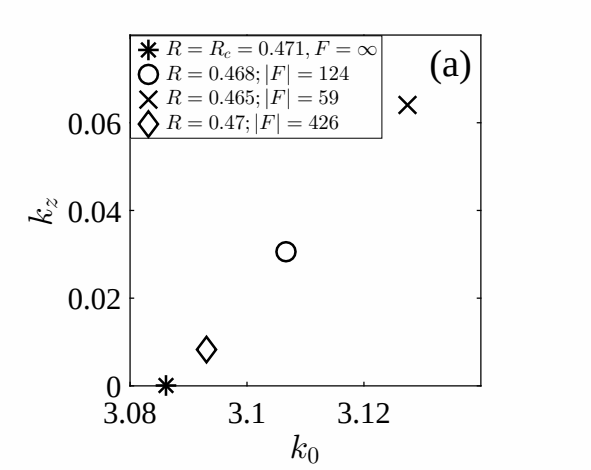

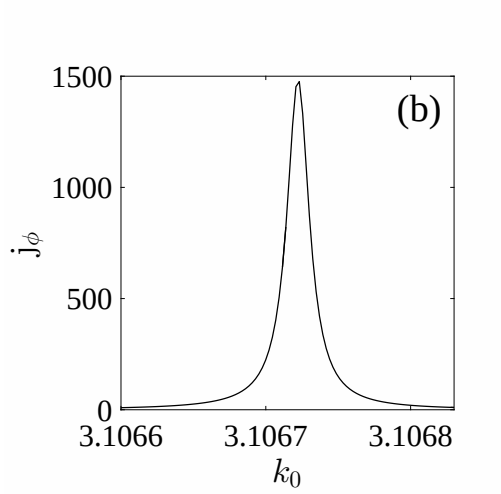

Figure 7: (a) Values of the enhancement factor $|F|$ vs k_z and k_0 as dependent on radius of spheres. (b) Value of the angular component of Poynting current for the $r = 0.571$ close to parameters of the BSC with OAM $m = 2$ (27). $k_z = 0.0303$.

to create giant spinning Poynting currents [51] as demonstrated in Fig. 7 (b). Fig. 8 shows as the giant Poynting current circulates around the array when the light with polarization $\alpha = -0.3133 + i0.9496$ and angle of incidence $\beta = 0.0306$ illuminates the array illustrating transformation of SAM into OAM.

9. Discussions and summary

Recently the BSCs above the light cone were shown to exist in various systems of one-dimensional arrays of dielectric rods and holes in the dielectric slab [12, 14, 13, 20, 22, 21, 15, 17] and of dielectric spheres [31]. In the present paper we chose another strategy to quantize the radiation continuum. We break a continual translational symmetry of infinitely long single rod along its axis z. In particular we have substituted the infinitely long circular rod by periodic array of dielectric spheres that allowed us to use the Mie scattering theory for a single sphere complemented with multiple events of mutual scattering processes

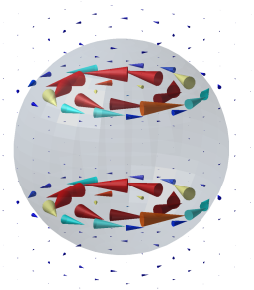

Figure 8: Poynting current circulates around the sphere when circularly polarized light illuminates the array. Currents around other spheres are repeating periodically.

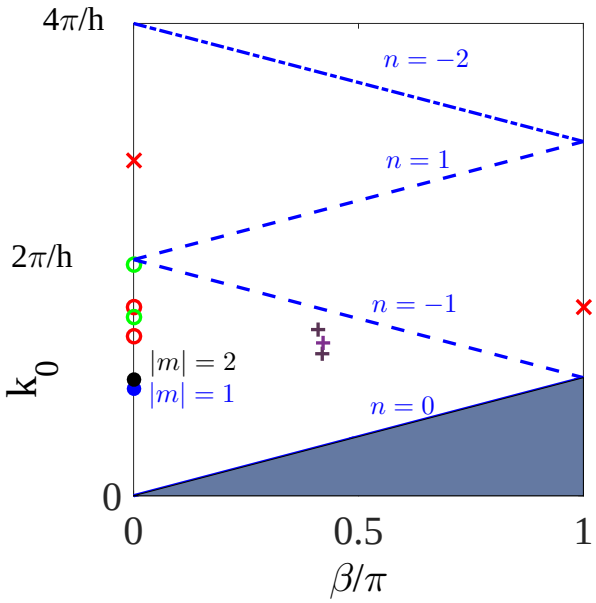

Figure 9: (Color online). BSC frequencies and Bloch vector β relative to the light line $k_0 = \beta$. The area filled by gray corresponds to below the light cone. Dash and dash-dot lines show thresholds where the next continua $n = \pm 1$ and $n = -2$ are opened. Fully symmetry protected BSCs are marked by open circles, two OAM BSCs with $m = \pm 1$ and $m = \pm 2$ are marked by closed circles, Bloch BSCs whose Bloch vector and frequencies are given for $\epsilon = 9, 11, 15$ and $R = 0.49$ are marked by '+', BSCs embedded into two and three continua are marked by crosses.

between spheres. Such a theory was developed recently by Linton *et al* [11] for guided electromagnetic modes below the light cone which shown by gray color in Fig. 9. As soon as the continual translational symmetry along the z-axis is substituted by discrete one the continua is quantized specified by two quantum numbers, magnetic quantum number

m and n. The last quantum number leads to discrete directions of outgoing cylindrical waves from the array given by the wave vector $k_{z,n} = \beta + 2\pi n/h$ in each sector m where β is the Bloch vector along the array.

We have performed symmetry analysis of the BSCs which are listed in tables I and II. The BSCs are labelled by two quantum numbers m, azimuthal number of continuum and β which defines Bloch wave vector of the BSC solution along the array. (1) The symmetry protected BSCs constitute the vast majority of BSCs which are symmetry mismatched with the first diffraction continuum $m = 0, n = 0$ of both polarizations. The EM field configurations of BSCs presented in Fig. 4 show hybridizations of a few orbital quantum numbers $l = 2, 4, 6, \ldots$ that specifies the BSCs as multipoles of high order. The most remarkable property in view of experimental visualization of the BSCs is their robustness relative to choice of material parameters of the dielectric spheres, the radius and dielectric constant.

(2) We demonstrated that the BSC can be established not only by variation of the material parameters but also by variation of Bloch wave vector β along the array axis. Patterns of the Bloch BSCs are presented in Fig. 3.

(3) The advantages of dielectric structures are a high quality factor and a wide range of BSC wavelengths from microns (photonics) to centimeter (microwave range) as dependent on the choice of the radius of the spheres. Although the BSCs exist in selected points in the parametric space, radius and dielectric constant there is a domain in the vicinity of the BSC point where the BSC mostly contributes into the cross-section and the EM field in the near field zone as shown in Figs. 5. That leads to extremely efficient light harvesting capabilities [52]. The BSCs with OAM $m \neq 0$ demonstrate the most striking effect of transformation of incident SAM beam with elliptic polarization into the OAM solution with giant spinning Poynting current in the near field zone of the array. It is worthy to note that the direction of current circulation can be easily inverted by changing the angle of incidence.

(4). There is a difference between the present theory and possible experimental realization of the BSCs that is a finite number of the spheres. There are also material losses and the spheres have fluctuations in shape because of technological reasons. All these factor transform the BSCs into quasi-BSCs with finite line width. For the fluctuations of the radius $\langle \Delta R^2/R^2 \rangle = 10^{-4}$ we have the inhomogeneous line width of order 0.01. Our numerics give the line width 0.003 as shown in Fig. 10 by dash line. Also Fig. 10 shows that for this case there is no necessity to include extremely large number of spheres because the inhomogeneous line width becomes more important factor compared to effect of finite number of the spheres with increasing of the number of the spheres.

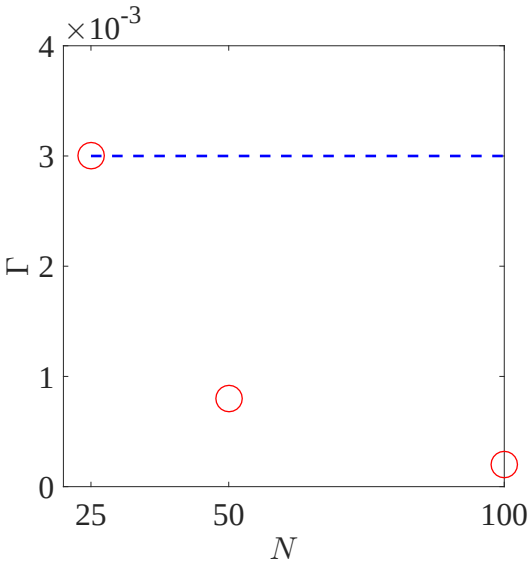

Figure 10: The line widths of the quasi-BSCs vs the number of spheres. Dash line shows the line width caused by fluctuations of the sphere's radiuses with dispersion $\sqrt{\langle \Delta R^2/R^2 \rangle} = 10^{-2}$.

Acknowledgement

The work was supported by Russian Science Foundation through grant 14-12-00266. We acknowledge discussions with D.N. Maksimov.

References

[1] A. Quirantes, F. Arroyo, and J. Quirantes-Ros, "Multiple Light Scattering by Spherical Particle Systems and Its Dependence on Concentration: A T-Matrix Study," J. Colloid and Interface Sc., vol. 240, pp. 78–82, 2001. doi:10.1006/jcis.2001.7641.

[2] Pi-Gang Luan, Kao-Der Chang, "Transmission characteristics of finite periodic dielectric waveguides," Opt. Express, vol.14, No. 8, pp. 3263–3272, 2006. doi: 10.1364/OE.14.003263.

[3] R. Zhao, T. Zhai, Z. Wang, and D. Liu, "Guided Resonances in Periodic Dielectric Waveguides," J. Lightwave Tech., vol. 27, No. 20, pp. 4544–4547, 2009. 10.1109/JLT.2009.2024629.

[4] J. Du, S. Liu, Z. Lin, J. Zi, and S.T. Chui, "Guiding electromagnetic energy below the diffraction limit with dielectric particle arrays," Phys. Rev. A, vol. 79, nO. 5, p. 051801R, 2009. DOI: 10.1103/PhysRevA.79.051801.

[5] A.L. Burin, H. Cao, G.C. Schatz and M.A. Ratner, "High-quality optical modes in low-dimensional arrays of nanoparticles: application to random lasers," J. Opt. Soc. A., vol. 21, No. 1, pp. 121–131, 2004.

[6] M. Gozman, I. Polishchuk, and A. Burin, "Light propagation in linear arrays of spherical particles," Phys. Lett. A, vol. 372, No. 31, pp. 5250–5253, 2008. doi: 10.1016/j.physleta.2008.05.084

[7] G.S. Blaustein, M.I. Gozman, O. Samoylova, I.Ya. Polishchuk, A.L. Burin, "Guiding optical modes in

chains of dielectric particles," Opt. Express, vol. 15, No. 25, pp. 17380–17391, 2007.

[8] B.T. Draine and P.J. Flatau, "Discrete-dipole approximation for periodic targets: theory and tests," J. Opt. Soc. Am. A, vol. 25, No. 11, pp. 2693–2703, 2008.

[9] R.S. Savelev, A.P. Slobozhanyuk, A.E. Miroshnichenko, Yu.S. Kivshar, and P.A. Belov, "Subwavelength waveguides composed of dielectric nanoparticles," Phys. Rev. B, vol. 89, No. 3, p. 035435, 2014. DOI: 10.1103/PhysRevB.89.035435.

[10] R. S. Savelev, S. V. Makarov, A. E. Krasnok, and P. A. Belov, "From Optical Magnetic resonance to dielectric nanophotonics," Optics and Spectroscopy, vol. 119, No. 4, pp. 551–568, 2015. DOI: 10.1134/S0030400X15100240.

[11] C.M. Linton, V. Zalipaev, and I. Thompson, "Electromagnetic guided waves on linear arrays of spheres," Wave Motion, vol.50, No. 1, pp. 29–40, 2013.

[12] S.P. Shipman and S. Venakides, "Resonant transmission near nonrobust periodic slab modes," Phys. Rev. E, vol. 71, No. 2, p. 026611, 2005.

[13] D. C. Marinica, A. G. Borisov, and S.V. Shabanov, "Bound States in the Continuum in Photonics," Phys. Rev. Lett., vol. 100, No. 18, p. 183902, 2008. DOI: 10.1103/PhysRevLett.100.183902.

[14] R.F. Ndangali and S.V. Shabanov, "Electromagnetic bound states in the radiation continuum for periodic double arrays of subwavelength dielectric cylinders," J. Math. Phys., vol. 51, No. 10, p. 102901, 2010. doi:10.1063/1.3486358.

[15] E.N. Bulgakov and A.F. Sadreev, "Bloch bound states in the radiation continuum in a periodic array of dielectric rods, Phys. Rev. A, vol. 90, No. 5, p. 053801, 2014. DOI: 10.1103/PhysRevA.90.053801.

[16] M. Song, H. Yu, C. Wang, N. Yao, M. Pu, J. Luo, Z. Zhang, and X. Luo, "Sharp Fano resonance induced by a single layer of nanorods with perturbed periodicity," Opt. Express, vol. 23, No. 3, pp. 2895–2903, 2015.

[17] Zhen Hu and Ya Yan Lu, "Standing waves on two-dimensional periodic dielectric waveguides," J. Optics, vol. 17, No. 6, p. 065601, 2015.

[18] Lijun Yuan and Ya Yan Lu, "Diffraction of plane waves by a periodic array of nonlinear circular cylinders," Phys. Rev. A, vol. 94, No. 13, p. 013852 (2016). DOI: 10.1103/PhysRevA.94.013852.

[19] J. Lee, B. Zhen, S.-L. Chua, W. Qiu, J.D. Joannopoulos, M. Soljačić, and O. Shapira, "Observation and Differentiation of Unique High-Q Optical Resonances Near Zero Wave Vector in Macroscopic Photonic Crystal Slabs," Phys. Rev. Lett., vol. 109, No. 6, p. 067401, 2012.

[20] C.W. Hsu, B. Zhen , Song-Liang Chua , S.G. Johnson, J.D.Joannopoulos, and M. Soljačić, "Bloch surface eigen states with in the radiation continuum, Light: Science and Applications, vol. 2, pp. 1–5, 2013. doi:10.1038/lsa.2013.40.

[21] Y. Yang, C. Peng, Y. Liang, Z. Li, and S. Noda, "Analytical Perspective for Bound States in the Continuum in Photonic Crystal Slabs," Phys. Rev. Lett. vol. 113, No. 3, p. 037401, 2014. DOI: 10.1103/PhysRevLett.113.037401.

[22] Bo Zhen, Chia Wei Hsu, Ling Lu, A.D. Stone, and M. Soljačić, "Topological Nature of Optical Bound States in the Continuum," Phys. Rev. Lett., vol. 113, No. 25, 257401, 2014. DOI: 10.1103/PhysRevLett.113.257401.

[23] M. Zhang and X. Zhang, "Ultrasensitive optical absorption in graphene based on bound states in the continuum," Scientific Rep., vol. 5:8266, pp. 1–6, 2015. DOI:10.1038/srep08266.

[24] J. von Neumann and E. Wigner, ""Uber merkwüdige diskrete eigenwerte," Z. Physik, vol. 50, pp. 291–293, 1929.

[25] Y. Plotnik, O. Peleg, F. Dreisow, M. Heinrich, S. Nolte, A. Szameit, and M. Segev, "Experimental observation of optical bound states in the continuum," Phys. Rev. Lett., vol. 107, No. 18, p. 183901, 2011. DOI: 10.1103/PhysRevLett.107.183901.

[26] M. López-García, J.F. Galisteo-López, C. López, and A. García-Martín, "Light confinement by two-dimensional arrays of dielectric spheres," Phys. Rev. B, vol. 85, No. 23, p. 235145, 2012.

[27] G. Corrielli, G. Della Valle, A. Crespi, R. Osellame, and S. Longhi, "Observation of surface states with algebraic localization," Phys. Rev. Lett., vol. 111, No. 22, p. 220403, 2013. DOI: 10.1103/PhysRevLett.111.220403.

[28] S. Weimann, Yi Xu, R. Keil, A.E. Miroshnichenko, A. Tünnermann, S. Nolte, A.A. Sukhorukov, A. Szameit, and Yu.S. Kivshar, "Compact surface fano states embedded in the continuum of waveguide arrays, Phys. Rev. Lett., vol. 111, No. 24, p. 240403, 2013. DOI: 10.1103/PhysRevLett.111.240403.

[29] Chia Wei Hsu, Bo Zhen, A.D. Stone, J.D. Joannopoulos, and M. Soljačić, "Bound states in the continuum," Nature Rev. Mater., Advance Online Publication 1, p. 16048, (2016). DOI: 10.1038/natrevmats.2016.48

[30] J. A. Stratton, *Electromagnetic Theory*, McGraw-Hill, New York, 1941.

[31] E.N. Bulgakov and A.F. Sadreev, "Light trapping above the light cone in one-dimensional array of dielectric spheres," Phys. Rev. A, vol. 92, No. 2, p. 023816, 2015. DOI: 10.1103/PhysRevA.92.023816.

[32] J.H. Bruning and Y.T. Lo, "Multiple scattering of EM waves by spheres Part I - multipole expansion and ray-optical solutions," IEEE Trans. Antennas and Propagation, vol. AP-19, No. 3, pp. 378–390, 1971.

[33] R. Porter and D.V.Evans, "Embedded Rayleigh–Bloch surface waves along periodic rectangular arrays," Wave Motion, vol. 43, pp. 29–50, 2005.

[34] K. Ohtaka, "Scattering theory of low-energy photon diffraction," J. Phys. C: Solis State Phys., vol. 13, pp. 667–680, 1980.

[35] K.A. Fuller and G.W. Kattawar, "Consummate solution to the problem of classical electromagnetic scattering by an ensemble of spheres. I: Linear chains," Opt. Lett., vol. 13, pp. 90–92, 1988.

[36] Yu-lin Xu, "Electromagnetic scattering by an aggregate of spheres," Appl. Optics, vol. 34, No. 21, pp. 4573–4588, 1995.

[37] A.-S. Bonnet-Bendhia and F. Starling, "Guided waves by electromagnetic gratings and non uniqueness examples for the diffraction problem," Math. Methods Appl. Sci. **17**, 305 (1994).

[38] A.F. Sadreev, E.N. Bulgakov, and I. Rotter, "Bound states in the continuum in open quantum billiards with a variable shape," Phys. Rev. B, vol. 73, No. 23, p. 235342, 2006. DOI: 10.1103/PhysRevB.73.235342.

[39] E. N. Bulgakov , K. N. Pichugin , A. F. Sadreev , and I. Rotter, "Bound States in the Continuum in Open AharonovBohm Rings," JETP Lett., vol. 84, No. 8, pp. 430–435, 2006. DOI: 10.1134/S0021364006200057.

[40] N. Bulgakov, I. Rotter,1 and A. F. Sadreev, "Comment on Bound-state eigenenergy outside and inside the continuum for unstable multilevel systems, Phys. Rev. A **75**, 067401 (2007).

[41] J.D. Jackson, *Classical Electrodynamics*, N.Y., 1962.

[42] Li Jun Yuan and Ya Yan Lu, "Propagating Bloch modes above the lightline on a periodic array of cylinders", J. Opt. Soc. Am. (2016).

[43] E.N. Bulgakov and D.N. Maksimov, "Light guiding above the light line in arrays of dielectric nanospheres", Opt. Lett. **41**, 3888 (2016).

[44] A. F. Sadreev and I. Rotter, "S-matrix theory for transmission through billiards in tight-binding approach," J. Phys. A: Math. Gen., vol. 36, pp. 11413–11433, 2003.

[45] L. Allen, M.W. Beijersbergen, R.J.C. Spreeuw, and J.P. Woerdman, "Orbital angular momentum of light and the transformation of Laguerre-Gaussian laser modes," Phys. Rev. A, vol. 45, No. 11, 8185–8189, 1992.

[46] L. Allen, M.J. Padgett, "The Poynting vector in Laguerre-Gaussian beams and the interpretation of their angular momentum density," Opt. Comm., vol. 184, pp. 67–71, 2000.

[47] A.M. Yao and M.J. Padgett, "Orbital angular momentum: origins, behavior and applications," Adv. Opt. Photon. vol. 3, pp. 161–204, 2011. doi:10.1364/AOP.3.00016.

[48] M. Berezin, E. O. Kamenetskii, and R. Shavit, "Magnetoelectric-field microwave antennas: Far-field orbital angular momenta from chiral-topology near fields," arXiv preprint: 1512.01393, 2015.

[49] Yu. Gorodetski, A. Drezet, C. Genet, and T.W. Ebbesen, "Generating Far-Field Orbital Angular Momenta from Near-Field Optical Chirality," Phys. Rev. Lett., vol. 110, No. 20, p. 203906, 2013.

[50] N. Yu, F. Capasso, "Optics with designer metasurfaces," Nature Mat. vol. 13, pp. 139–150, 2014. DOI: 10.1038/NMAT3839.

[51] E. N. Bulgakov and A. F. Sadreev, "Giant optical vortex in photonic crystal waveguide with nonlinear optical cavity," Phys. Rev. B, vol. 85, No. 16, 165305, 2012. DOI: 10.1103/PhysRevB.85.165305.

[52] A. I. Fernandez-Dominguez, S.A. Maier, and J. B. Pendry, "Collection and Concentration of Light by Touching Spheres: A Transformation Optics Approach," Phys. Rev. Lett., vol. 105, No. 26, p. 266807, 2010.